# High resolution spectroscopic investigation of the CH 2 CHO radical in the sub-millimeter region

Rosemonde Chahbazian, Marie-Aline Martin-Drumel, Olivier Pirali

# High resolution spectroscopic investigation of the $CH_2CHO$ radical in the sub-millimeter region

Rosemonde Chahbazian, Marie-Aline Martin-Drumel, and Olivier Pirali*

*Université Paris-Saclay, CNRS, Institut des Sciences Moléculaire d'Orsay, 91400 Orsay, France*

E-mail: rosemonde.chahbazian@universite-paris-saclay.fr

**Abstract**

In this work, the pure rotational spectrum of the vinoxy radical ($CH_2CHO$) has been studied at millimeter- and sub-millimeter wavelengths (110–860 GHz). $CH_2CHO$ was produced by H abstraction from acetaldehyde ($CH_3CHO$) using atomic fluorine in a double-pass absorption cell at room temperature. A Zeeman-modulation spectrometer, in which an external magnetic field generated inside the absorption cell is amplitude modulated, has been used to record the pure rotational transitions of the radical. The recorded spectra are devoided of signals from closed-shell species, allowing relatively fast acquisitions over wide spectral windows. Transitions involving values of the rotational quantum numbers $N''$ and $K_a''$ up to 41 and 18, respectively, were measured and combined with all available high-resolution literature data (both pure rotation and ground state combination differences from ro-vibration) to greatly improve the modeling of the $CH_2CHO$ spectrum. The combined experimental linelist is fit using a semi-rigid rotor Hamiltonian and the results are compared to quantum chemical calculations. This laboratory study provides the spectroscopic information needed to search for $CH_2CHO$ in various interstellar environments, from cold (e.g., typically 10 K for dense molecular clouds) to warm (e.g., $\sim$ 200 K for hot corinos) objects.

# Introduction

Radicals are key species for chemical reactions occurring in combustions, atmospherical and astrophysical environments[1,2]. As a primary product of the reaction between oxygen and olefins—as ethylene—of relevance for combustion processes, the vinoxy ($CH_2CHO$) radical has attracted much interest (see, e.g., Refs.[3–5]). In astrophysical environments, the oxidation reaction of $C_2H_4$ has been proposed to lead to the production of $CH_2CHO$ with a 30% yield in high-temperature sources such as hot cores ($\sim 200 - 300$ K)[6]. The unambiguous interstellar detection and column density determination of $CH_2CHO$, whose structure is represented in Fig. 1, would validate this model. However, the radical remains elusive in the ISM, preventing a deep understanding of its formation route and reactivity in outer space.

Spectroscopic investigations on $CH_2CHO$ were initiated by the observation of the $\tilde{B}$–$\tilde{X}$ band of the radical by Ramsay[7], subsequently investigated by Inoue and Akimoto[8]. The later study was rapidly followed by infrared vibrational spectroscopy in Ar isolated matrix[9], which included an isotopic substitution of the precursor to support the vibrational band assignments in the ground electronic state. The first rotationally-resolved spectra were obtained for the $\tilde{B}$–$\tilde{X}$ band by Heaven et al.[10] and DiMauro et al.[11] using laser-induced fluorescence spectroscopy, providing insights into the rotational structure and spin splittings of the radical. Other studies focused on the $\tilde{B}$–$\tilde{X}$[12–15] and $\tilde{A}$–$\tilde{X}$[3,16–18] electronic bands. Using millimeter-wave spectroscopy, the pure rotational spectrum of $CH_2CHO$ was first observed by Endo et al.[4]. At these wavelengths, the hyperfine structure was resolved for the two protons (but not for the third proton, noted $H_3$ hereafter, of the –CHO moiety, see Fig. 1). Because only $a$-type transitions were observed in that work, the $K$ dependant centrifugal distortion constant $\Delta_K$ could not be determined. In what remains today the only high-resolution vibrational investigation of the radical, Utkin et al.[19] recorded the rotationally-resolved spectrum of the $\nu_3$ band around 2800 cm$^{-1}$. From the assigned $b$-type transitions, the authors were able to manually adjust (but not fit) the value of the $\Delta_K$ constant in the ground state. Hansen et al.[20] pursued the investigation of the rotational spectrum of $CH_2CHO$ in the microwave domain but their assignments are in disagreement with those subsequently reported by

Endo and Nakajima[21]. In the latter study, four *b*-type rotational lines were also measured which led to a significant refinement of the $A$ rotational constant while keeping the $\Delta_K$ fixed to the value determined by Utkin et al.[19].

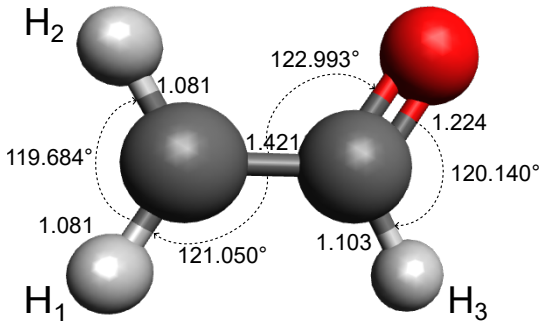


Figure 1: **Representation of the structure of $CH_2CHO$**. The numbering of the three protons—$H_1$, $H_2$ and $H_3$—is indicated. The values of the distances (in Å) and angles (in degrees) are those derived from our calculations.

As a model molecule for resonant structures, the vinoxy radical has been the subject of discussions in the literature. Indeed, it possesses two isoelectronic structures: the formyl methyl structure (involving a C=O bond, $^{\bullet}CH_2CH{=}O$) and the ethenyloxy—or vinoxy—structure (involving a C=C bond, $CH_2{=}CHO^{\bullet}$). These two forms are indistinguishable because of electronic resonance $CH_2CHO$ (see, e.g., Ref.[8]), but many literature studies have aimed at determining the dominant nature. In the ground electronic state, it is now well-established that the formyl methyl resonance form is dominant (although the common name of the radical remains vinoxy): it was predicted by calculations (see, e.g., Refs.[22,23]) and confirmed by experiments by Jacox[9] using isotopic substitutions and by Endo et al.[4] using the hyperfine coupling constants of the protons. The structural parameters of the skeleton were first determined by DiMauro et al.[11] using electronic spectroscopy and then by Endo and Hirota[24] using isotopic substitution millimeter-wave spectroscopy.

In the literature, high-resolution pure rotational data are limited to relatively low values of the rotational quantum numbers ($N_{\max} = 7$ and $K_{a\,\max} = 5$ in the work from Endo et al.[25] between 81 and 176 GHz). The observed transitions allow the search for the yet-to-be-detected vinoxy radical in cold sources of the interstellar medium using highly sensitive millimeter-wave radiotelescopes

(such as NOEMA[26] and ALMA[27]). However, high-resolution measurements covering a broader spectral range and involving higher values of $N$ and $K_a$ are mandatory to search for this intermediate species in warmer environments, such as hot cores, knowing that at higher temperatures the most intense lines are around 176 GHz. In the present work, we recorded the high-resolution spectrum of $CH_2CHO$ in a spectral range spanning from 140 to 850 GHz. Most of the observed transitions are $a$-type transitions involving values of $N''$ and $K_a''$ up to 41 and 18, respectively, while $b$-type transitions involve values of $N''$ and $K_a''$ up to 22 and 3, respectively. These new observations allow a significant refinement of the model describing the rotational structure of the lowest vibronic state of the radical and enable interstellar searches in the sub-millimeter domain.

The paper is built as follows: the performances of our experimental set-up, which allows for efficiently broad spectral recordings of radicals lines, is described in the following section; the results of the spectral analysis as well as the comparison of our model with the literature are given in the second section; astronomical implications are discussed in the last section.

# Laboratory methods

## Quantum chemical calculations

Geometry optimization and anharmonic frequency analysis have been carried out at the $\omega$B97X-D/cc-pVQZ level of theory[28–30] using the Gaussian 16 suite of electronic structure programs[31]. The resulting equilibrium structural parameters of $CH_2CHO$ are reported in Fig. 1.

## Synthesis of $CH_2CHO$

Inoue and Akimoto[8] and Endo et al.[25] have shown that H-abstraction from acetaldehyde ($CH_3CHO$) by F atoms (themselves synthesized by a microwave discharge in $CF_4$) leads to a relatively abundant production of $CH_2CHO$ radicals. These authors observed that this synthesis technique yields a radical concentration five times larger than that obtained by the reaction of ethylene ($C_2H_4$) with oxygen atoms. We applied a similar technique in our work, replacing $CF_4$

with a mixture of $F_2$ diluted in He (5 % dilution) similar to what we previously used to study the $CH_2OH$[32,33] and $CH_2CN$[34] radicals in the sub-millimeter region. The technique has proven to be very efficient in selectively producing the targeted paramagnetic species. The details of the reaction cell design are given in Ref.[34]. Shortly, this cell is a two-meter-long Pyrex tube with its internal surface covered by a fluorinated wax and equipped with three F injection inlets. The optical configuration allows for a double pass of the radiation in the cell, although in this study the spectra in the 140–220 GHz range were recorded in a single pass configuration (higher frequency transitions were acquired in a double pass configuration). The signal of $CH_2CHO$ was optimized on the transition centered at 153785.5 MHz, originally measured by Endo et al.[25]. The optimum signal was obtained with about 40 µbar of $CH_3CHO$ and 50 µbar of the $F_2$/He mixture, measured in a continuous gas flow maintained by a roots blower.

## Zeeman Modulated (Sub-)millimeter Spectrometer

In the present work, the transitions of $CH_2CHO$ were recorded using a (sub-)millimeter wave spectrometer previously described in Chitarra et al.[34]. It consists of a frequency multiplication chain (from Virginia Diode Inc.) fed by the RF frequency of a synthesizer (Rhode & Schwarz) for which a 10 MHz reference signal is provided by a Rubidium clock (Stanford Research). We used Schottky diode detectors (VDI) to measure the transitions in the 140–220 GHz and 220–330 GHz spectral ranges and a mechanically-cooled Indium antimonide (InSb) bolometer (QMC) between 330 GHz and 850 GHz. The main difference between the present study and our previous works[32–34] is that instead of a source frequency modulation (FM) or a double modulation (FM together with Zeeman modulation[35]), a single Zeeman modulation (ZM) scheme was used here. This was achieved using an alternating magnetic field generated by an 18 A alternating current (AC) circulating in a coil surrounding the cell (about 400 spirals/m, with a total resistance of about 5.5 Ω). The sinusoidal signal was generated by a waveform generator operating at 16.9 kHz followed by an audio amplifier providing the required current to obtain a 14.5 Gauss magnetic field. As the entire sinusoidal waveform feeds the coil (no rectification nor half-rectification of the AC signal), the

rotational levels of open-shell species are split by the Zeeman effect twice per modulation period. The detection is performed using a phase-sensitive lock-in amplifier for which the reference signal is the magnetic field modulation frequency (demodulation at the first harmonic). The frequency steps ranged from 100 to 500 kHz according to the Doppler line broadening and the time constant was adjusted to values ranging from 20 ms to 2 s depending on the line intensity. The line frequency accuracy varies from 50 to 200 kHz in these conditions.

Traditionally when investigating radicals in the (sub-)millimeter range, acquisitions are mostly made line-by-line. Here, the ZM detection scheme allows probing wide spectral windows (typically 1–10 GHz) relatively fast, with good SNR and almost no interference from precursor lines. For example, a spectral survey of the 335 GHz to 385 GHz range, showing the achievable broad spectral coverage, is given on the upper panel of Fig. 2. The 50 GHz were recorded with 30 ms per point and 200 kHz frequency steps resulting in a relatively fast acquisition (of about 10 hours for the full range plotted in the upper panel in Fig. 2). Additionally, specific portions of the spectrum, where transitions of $CH_2CHO$ were expected, were recorded with deeper integration conditions. For example, the portion of the spectrum displayed in the lower panel of Fig. 2 was recorded with an acquisition time of 300 ms/point and 100 kHz frequency steps (150 minutes acquisition time). Hundreds of lines of the $CH_2CHO$ radical are detected with a signal-to-noise ratio (SNR) greater than 10 for the most intense lines. This survey also identified numerous lines of HCO radical with good SNR. These lines are shown on the lower panel of Fig. 2, where we compare the experimental spectrum with the predictions of HCO (using the catalog from the JPL database[36]) and our prediction of $CH_2CHO$ lines at 300 K.

# Results and discussion

## Spectroscopic Description

The vinoxy radical is a near-prolate asymmetric top molecule[14] with a $^2$A" electronic ground state[22]. The two permanent dipole moments lie along the $a$-axis and $b$-axis of inertia and take

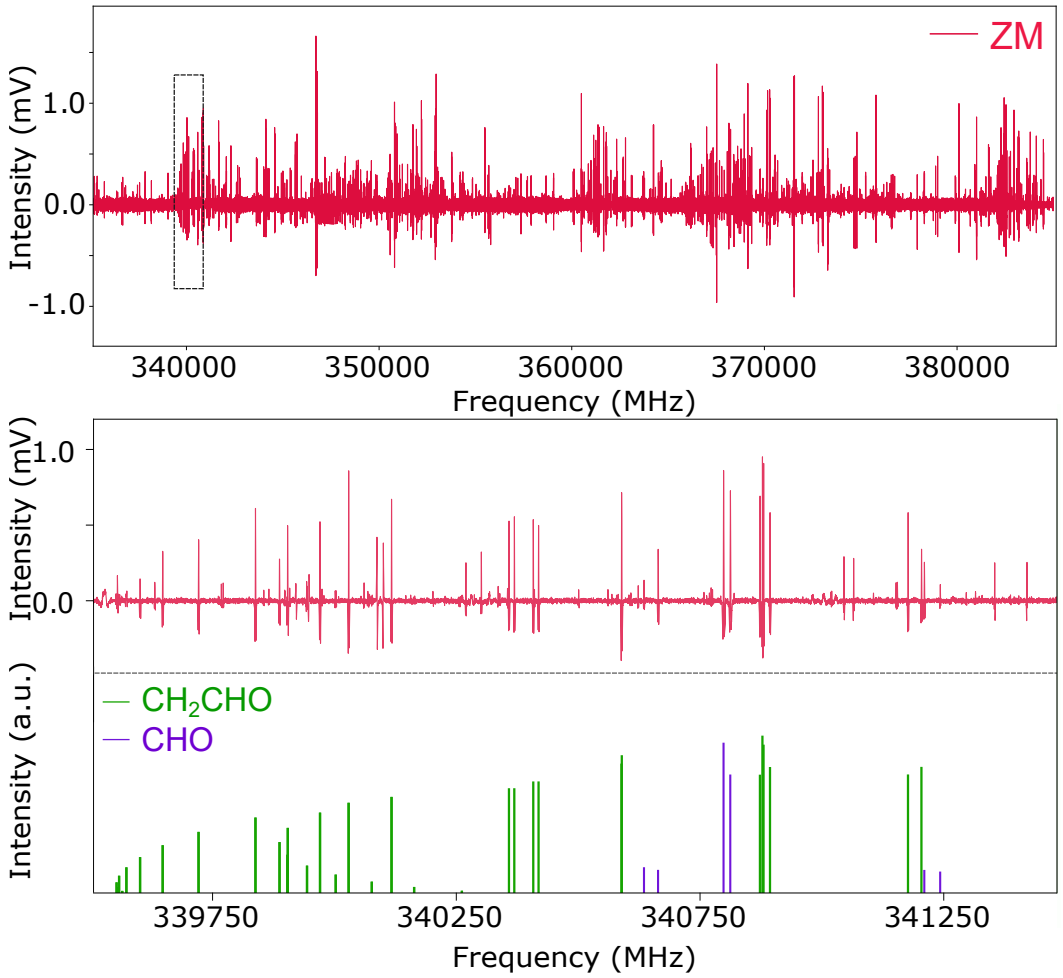


Figure 2: **Portion of the experimental spectrum recorded with ZM.** The top trace shows the survey from 335 to 385 GHz, where numerous lines are detected. Thanks to the use of ZM, no saturation of the precursor lines is observed. Only lines from radical species appear in the spectrum. The lower trace shows the region of the $N'' = 16$ $a$-type cluster of transitions of the $CH_2CHO$ radical (in green) simulated with the final set of spectroscopic parameters obtained in this work (see later in text). Strong lines of the CHO radical are shown in purple (frequencies extracted from the JPL database[36]). Residual lines may belong to vibrational satellites of these two radicals or to the $CH_3CO$ radical also synthesized in this experiment (analysis in progress).

values of $\mu_a = 2.76$ Debye and $\mu_b = 0.92$ Debye[21]. $CH_2CHO$ has three nonequivalent protons and one unpaired valence electron. The Hamiltonian employed to model the energy levels of the vibronic ground state is built as follows (1):

$$\hat{H} = \hat{H}_{\text{rot}} + \hat{H}_{\text{sr}} + \hat{H}_{\text{hfs,1}} + \hat{H}_{\text{hfs,2}} + \hat{H}_{\text{hfs,3}} \tag{1}$$

where $\hat{H}_{\text{rot}}$ refers to the rotational Hamiltonian, $\hat{H}_{\text{sr}}$ refers to the spin-rotation Hamiltonian involving the unpaired electron, and $\hat{H}_{\text{hfs,1}}$, $\hat{H}_{\text{hfs,2}}$ and $\hat{H}_{\text{hfs,3}}$ are the hyperfine structure Hamiltonian accounting for the non-zero nuclear spin of the three protons $H_1$, $H_2$ and $H_3$, with $I_{H_1} = I_{H_2} = I_{H_3} = 1/2$ (see Fig. 1). The standard $N$, $K_a$, and $K_c$ quantum numbers label the rotational levels. Due to the electron spin-rotation coupling, each level is split into two $J$ sub-levels, with $\mathbf{J} = \mathbf{N} + \mathbf{S}$ ($S = 1/2$). Then, each sub-level is further split into hyperfine sub-levels because of the spin-spin coupling of the three hydrogens. This leads to sixteen hyperfine sub-levels as the three protons are non-equivalent. Each sub-level is labeled using the $F_1$, $F_2$ and $F$ quantum numbers, defined as : $\mathbf{F_1} = \mathbf{J} + \mathbf{I}_{H_1}$, $\mathbf{F_2} = \mathbf{F_1} + \mathbf{I}_{H_2}$ and $\mathbf{F} = \mathbf{F_2} + \mathbf{I}_{H_3}$. In the present work, we partially resolved the hyperfine structure involving $H_1$ and $H_2$ because Doppler broadening limits the resolution. All lines were assigned using the PGOPHER program[37] and the fit was performed using the Pickett program[38].

## Performances of the Zeeman modulation scheme

The ZM method is well known to be efficient to study paramagnetic species, as described by Guelachvili[39]. If we compare a double modulation scheme (using FM followed by ZM, as implemented in Chitarra et al.[34]) with pure ZM at kHz modulation frequencies, ZM is advantageous because it allows filtering of the precursor lines (as well as of the lines of all the other closed-shell molecules produced in the experiment) which often saturates the lock-in amplifier and obliterates wide parts of the spectrum, preventing the observation of numerous paramagnetic lines. This is illustrated in Fig. 3 where three lines of $CH_3CHO$ are observed in FM and saturate the lock-in (black trace, upper panel). In such conditions, in the regions where the FM signal is saturated, a

FM + ZM detection scheme would result in the absence of any magnetic field-dependant signal at the second demodulation stage, preventing the observation of the underlying $CH_2CHO$ transitions. In contrast, a relatively fast single ZM detection scheme allows to easily retrieve the signal from the radical species (red trace, bottom panel). The signal-to-noise ratio (SNR) is the same for both methods at low frequencies. However, at high frequencies ($\sim$ 600 GHz), the amplitude of the magnetic field generated by our set-up is not sufficient to split the rotational transitions out of the Doppler line width by the Zeeman effect. This translates to a drastic loss of the spectrometer sensibility.

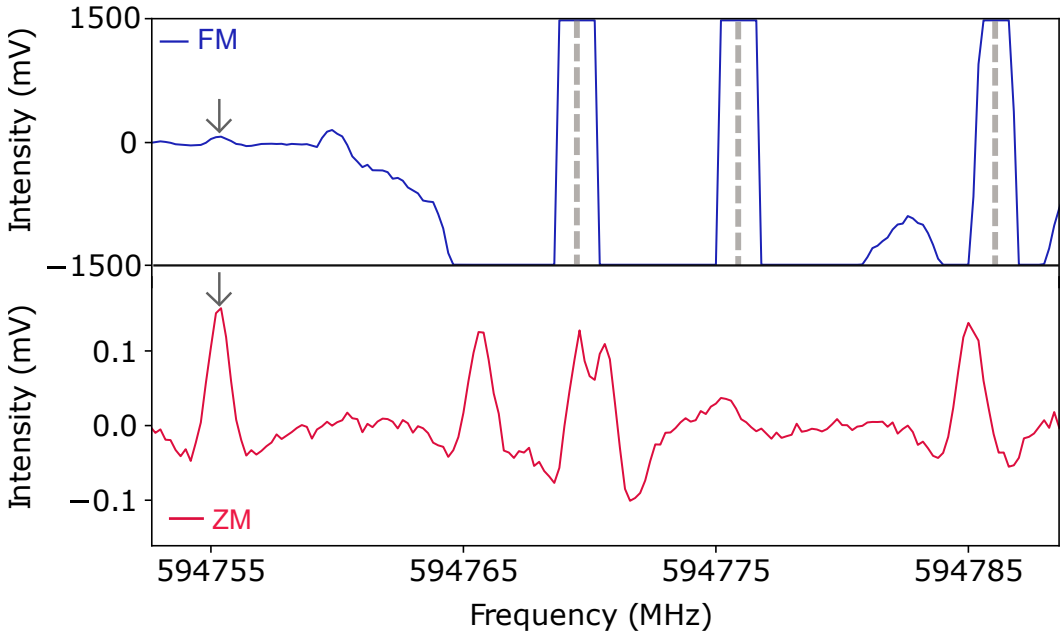


Figure 3: **Comparison between frequency modulation (FM, top trace) and Zeeman modulation (ZM, bottom trace)**. The FM spectrum shows three saturated lines for a lock-in sensitivity of 0.5 V, assigned to the $CH_3COH$ precursor. In a standard FM+ZM detection method, no information can be extracted around these three saturated lines and only one transition of $CH_2CHO$ is visible in the region plotted in the Fig. (the one marked with an arrow). The three precursor lines are well filtered in a pure ZM technique, revealing weaker paramagnetic lines assigned to $CH_2CHO$. Here, the acquisition time was 10 times longer for the ZM than for FM measurement because the Zeeman effect is less efficient in this range (see text).

## Spectroscopic analysis

Using the experimental set-up described above, we recorded large spectral surveys in the 110–860 GHz spectral range, avoiding spectral contamination of close-shell species as well as saturation issues of the lock-in amplifier. These portions of spectra allow us to perform a thorough characterization of the (sub-)millimeter wave spectra of the $CH_2CHO$ and $CH_3CO$ radicals, the latter being under analysis. We measured almost 3000 transitions of $CH_2CHO$, involving relatively high values of the rotational quantum numbers $N''$ and $K_a''$ up to 41 and 18 respectively.

We initiated this study by refitting the literature data using a Watson A-reduced Hamiltonian with the SPFIT program[38]. This data set contains all pure rotational transitions of Endo et al. [25] and Endo and Nakajima[21] with frequency errors ranging from 40 kHz to 400 kHz and 8 kHz to 80 kHz, respectively, based on the weights of the individual lines reported by the authors. In the set of parameters used to adjust the data, $\Delta_K$ was fixed to the value determined by IR spectroscopy[19]. All lines are reproduced within $5\sigma$ of their experimental accuracy, with a weighted standard deviation of 1.064 and an RMS of 59 kHz (see Table 1). However at $3\sigma$ rejection factor, the fit does not reproduce all lines of the literature, and 4 lines, at frequencies 95853.419 MHz, 81383.025 MHz, 42368.966 MHz, and 42357.564 MHz, are rejected (weighted standard deviation of 0.98 and RMS of 56.5 kHz). All parameters are in agreement with Endo and Nakajima[21], except for $T_{ab}(H_2)$ which is larger (see Table 1), probably due to the difference between the two models. Concerning $T_{ab}(H_3)$, when adjusted it takes the value of 1.51(72) MHz while not influencing the overall fit quality; we thus decided to remove it from the parameters at this stage.

We assigned 2960 rotational transitions (1013 different frequencies), mostly $a$-type R-branch transitions. The newly measured $a$-type lines involve values of $N''$ and $K_a''$ up to 41 and 18, respectively (against 7 and 5, respectively, in the previous study). The frequency uncertainties have been chosen based on the line width and the signal-to-noise ratio of each transition, ranging from 50 to 200 kHz. Up to about 500 GHz, many lines show partly resolved hyperfine structure (that results from the $H_1$ and $H_2$ atoms). Considering the large number of transitions with no hyperfine structure resolved, we introduced a 'dummy' vibrational state, without any hyperfine

splitting, in the model; this state is described with rotational, centrifugal distortion, and spin-rotation constants fixed to the values in the main hyperfine-split state. To reproduce all these transitions up to 850 GHz, we added only 10 parameters both for the rotation (all sextics diagonal terms with $\Phi_K$, $\phi_K$ and $\phi_{NK}$ fixed to the calculated values) and for the spin-rotation ($\Delta_N{}^s$, $\Delta_{KN}{}^s$ and $\delta_N{}^s$), which is a reasonable number of parameters comparing to the extension in $N''$ and $K_a''$ quantum numbers. Nevertheless, as the number of attributed $b$-type is low, we decided to include ground state combination difference (GSCD) from Utkin et al.[19] in the fit to improve the determination of $A$ and $\Delta_K$. We calculated 541 GSCD and their weights were attributed according to Utkin et al.[19] at 0.004 cm$^{-1}$ for transitions measured in the jet and at 0.006 cm$^{-1}$ for transitions measured at room temperature. This gives a fit with $\Delta_K$ taking the value of 1316.3(19) kHz, very close to the value estimated by Utkin et al.[19]. At that point, the fit reproduced all the rotational transitions and the GSCD at their experimental accuracy with a weighted standard deviation of 1.09 and an RMS of 98 kHz for the pure rotational data (with a factor rejection of $5\sigma$) and 0.0035 cm$^{-1}$ for the GSCD.

With this new set of spectroscopic parameters, we were able to search for $b$-type transitions in our surveys. We measured 59 $b$-type rotational transitions (32 different frequencies), between 210 GHz and 520 GHz, including 38 Q-branch transitions and 21 R-branch transitions. We did not measure $b$-type transitions at higher frequencies because above 500 GHz we performed mainly line-by-line acquisitions targeting the $a$-type transitions. The hyperfine structure of all $b$-type transitions was unresolved, except for four partially resolved transitions. Fig. 4 shows an example of such a partially resolved $b$-type transition. The splittings of the energy levels are due to the spin-spin coupling of $H_1$, $H_2$, and $H_3$ with the spin of the unpaired electron. Only the hyperfine structure due to $H_1$ and $H_2$ is resolved here.

Our final set of parameters shows better determination for all high-order terms of the rotational (quartics, sextics constants) and spin-rotation parameters ($\Delta_K{}^s$, $\Delta_N{}^s$, $\Delta_{KN}{}^s$ and $\delta_N{}^s$), in comparison with the literature values. By adding the $b$-type transitions to the fit, $\Delta_K$ takes the value 1313.10(13) kHz, and is 10 times better determined than previously. The values of the weighted

standard deviation and the RMS are respectively 0.81 and 80 kHz for Endo et al.[25], 1.63 and 14.02 kHz for Endo and Nakajima[21] and 1.07 and 102.8 kHz for the lines measured in this study. We note that the final experimental rotational, centrifugal distortion, and hyperfine parameters are in excellent agreement with the calculated ones. Larger discrepancies are seen with the spin-rotation parameters, although the fitted values remain in excellent agreement with the values derived by Endo and Nakajima[21].

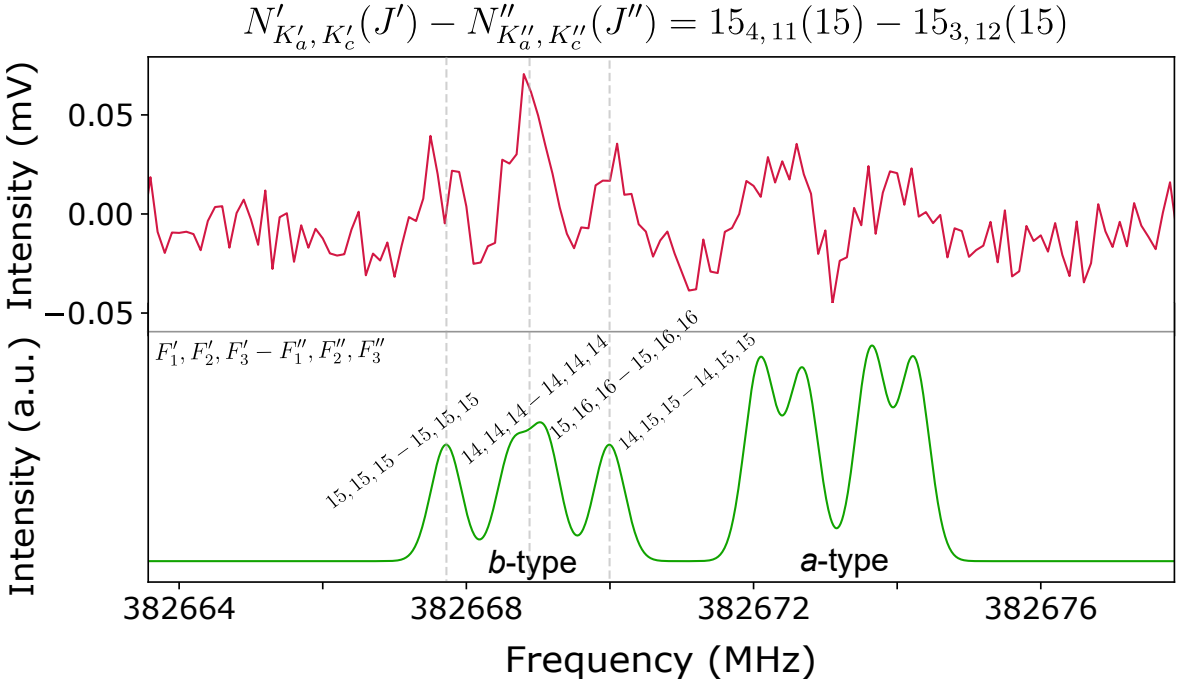


Figure 4: **Partially resolved hyperfine structure of a $b$-type transition of $CH_2CHO$.** The upper panel contains the experimental trace, and the lower panel is the simulated spectrum using the final set of spectroscopic parameters. Here the hyperfine structure is partially resolved, showing splittings due to the spin-spin interaction of $H_1$ and $H_2$ with the unpaired electron.

## Astronomical implications

The new set of spectroscopic parameters allows to accurately predict the rotational spectrum of $CH_2CHO$ from centimeter wavelengths up to 850 GHz. Such broad spectral coverage is crucial for light species as $CH_2CHO$ whose rotational spectrum extends to high frequencies, even under low-temperature conditions. For example, at temperatures relevant for hot corinos (e.g., $\sim$ 225 K[6]), the spectrum of $CH_2CHO$ peaks around 550 GHz (see Fig. 5, panel **a**). In this region, transitions

Table 1: Molecular constants for the vinoxy radical

| | units | Calculated [a] | Ref[21] | Refit Lit. | Exp. |
|---|---|---|---|---|---|
| $A$ | /MHz | 66856.48 | 66677.85679(159) | 66677.8578(17) | 66677.8581(13) |
| $B$ | /MHz | 11405.79 | 11447.0460(55) | 11447.0474(69) | 11447.04684(41) |
| $C$ | /MHz | 9743.53 | 9758.9065(53) | 9758.9050(68) | 9758.90748(36) |
| $\Delta_N$ | /kHz | 9.3427847 | 9.6468(22) | 9.642(28) | 9.67571(23) |
| $\Delta_{NK}$ | /kHz | −80.607172 | −83.045(137) | −83.01(17) | −83.1828(23) |
| $\Delta_K$ | /kHz | 1288.6753 | [1307.] | [1307.] | 1313.10(13) |
| $\delta_N$ | /kHz | 2.0122412 | 2.1215(101) | 2.169(14) | 2.09528(31) |
| $\delta_K$ | /kHz | 37.634069 | 38.4(26) | 38.3(33) | 40.669(15) |
| $\Phi_N$ | /Hz | 0.0167965 | | | 0.017303(99) |
| $\Phi_{NK}$ | /Hz | −0.00289155 | | | −0.0144(11) |
| $\Phi_{KN}$ | /Hz | −7.383695425 | | | −7.6141(83) |
| $\Phi_K$ | /Hz | 77.45606136 | | | [77.456061] |
| $\phi_N$ | /Hz | 0.007414007 | | | 0.00812(14) |
| $\phi_{NK}$ | /Hz | 0.084506752 | | | [0.084506752] |
| $\phi_K$ | /Hz | 13.43581186 | | | [13.435812] |
| $\epsilon_{aa}$ | /MHz | −969.18773 | −899.0720(63) | −899.0677(62) | −899.0777(51) |
| $\epsilon_{bb}$ | /MHz | −75.467329 | −66.2053(44) | −66.1975(47) | −66.1995(41) |
| $\epsilon_{cc}$ | /MHz | 3.1831907 | −0.6128(33) | −0.6150(35) | −0.6250(32) |
| $(\epsilon_{ab}+\epsilon_{ba})/2$ [b] | /MHz | −180.28534 | 84.0021(183) | 83.716(35) | 83.671(13) |
| ${\Delta_K}^s$ | /MHz | | 0.0385(32) | 0.0384(26) | 0.05216(35) |
| ${\Delta_N}^s$ | /MHz | | | | 0.0002448(37) |
| ${\Delta_{KN}}^s$ | /MHz | | | | 0.00375(14) |
| ${\delta_N}^s$ | /kHz | | | | 0.1519(43) |
| $a_F(\mathrm{H}_1)$ | /MHz | −53.04061 | −55.7658(48) | −55.7587(51) | −55.7517(47) |
| $T_{aa}(\mathrm{H}_1)$ | /MHz | 13.9884 | 11.9275(116) | 11.917(12) | 11.895(11) |
| $T_{bb}(\mathrm{H}_1)$ | /MHz | −13.7458 | −13.6902(118) | −13.700(12) | −13.717(12) |
| $T_{cc}(\mathrm{H}_1)$ [c] | /MHz | −0.2426 | | 1.783 | 1.822 |
| $T_{ab}(\mathrm{H}_1)$ [b] | /MHz | 29.917866 | −26.97(25) | −26.50(30) | −26.94(24) |
| $a_F(\mathrm{H}_2)$ | /MHz | −51.892733 | −54.1511(46) | −54.1548(49) | −54.1543(46) |
| $T_{aa}(\mathrm{H}_2)$ | /MHz | −29.8938 | −28.1502(78) | −28.1394(84) | −28.1364(79) |
| $T_{bb}(\mathrm{H}_2)$ | /MHz | 31.6087 | 28.3807(95) | 28.369(10) | 28.3687(97) |
| $T_{cc}(\mathrm{H}_2)$ [c] | /MHz | −1.7149 | | −0.2296 | −0.2323 |
| $T_{ab}(\mathrm{H}_2)$ [b] | /MHz | −5.5437919 | 4.91(25) | 8.30(67) | 8.36(38) |
| $a_F(\mathrm{H}_3)$ | /MHz | 1.3706762 | −0.5579(32) | −0.5563(34) | −0.5559(33) |
| $T_{aa}(\mathrm{H}_3)$ | /MHz | 3.6502 | 2.2312(78) | 2.2115(82) | 2.2031(78) |
| $T_{bb}(\mathrm{H}_3)$ | /MHz | 1.7105 | 2.7792(94) | 2.7989(99) | 2.8134(95) |
| $T_{cc}(\mathrm{H}_3)$ [c] | /MHz | −5.3607 | | −5.0104 | −5.0165 |
| $T_{ab}(\mathrm{H}_3)$ [b] | /MHz | −4.9996091 | 5.30(25) | | [−4.9996091] |
| $\#/n$ [d] | | | 585/567 | 585/567 | 4142/1774 |
| $N''_{\max}, K''_{a\max}$ | | | 7, 5 | 7, 5 | 41, 18 |
| RMS [e] | /MHz | | | 0.059 | 0.096 |
| RMS [f] | /cm$^{-1}$ | | | | 0.00323 |
| $\sigma$ [g] | | | | 1.064 | 1.012 |

[a] The calculated rotational constants have been Bayesian corrected by a 0.9866 factor (see Lee and McCarthy [40])

[b] The absolute sign cannot be retrieved in the fit (see Endo and Nakajima [21])

[c] Calculated from $T_{aa}+T_{bb}+T_{cc}=0$

[d] Number of lines (#) and number of lines with different frequencies ($n$), unitless

[e] Root mean square of the pure rotation data, in MHz

[f] Root mean square of the GSCD data [19], in cm$^{-1}$

[g] Weighted standard deviation, unitless

involve relatively large values of the $N''$ and $K_a''$ quantum numbers for which the predicting power of the model is often poor when the experimental dataset is limited (in terms of spectral coverage or probed quantum numbers). This deficiency in extrapolating accurate measurements to higher frequency is shown in the panels (**b**) and (**c**) of Fig. 5. Near 550 GHz, transitions involving $N'' = 24$ and $K_a'' = 4$ are relatively well predicted using the refit model which contains the literature dataset[21,25], with a shift between our measurements and the refit of the literature of the order of $\sim$ 1 MHz (see Fig. 5 **(b)**). However, for higher values of $N''$ (Fig. 5 **(c)**), the shift becomes much larger ($\sim$ 36 MHz), avoiding any possible interstellar detection of the radical at these frequencies.

## Conclusion and prospects

We have extended the investigation of the pure rotational spectrum of the $CH_2CHO$ radical, from 140 to 850 GHz. $CH_2CHO$ was produced from acetaldehyde, by hydrogen abstraction using fluorine atoms. We used a Zeeman-modulated spectrometer to record the data, allowing us to efficiently filter lines of the precursor that saturates the lock-in amplifier, obliterating a part of the spectrum, in conventional source-frequency modulated spectroscopy. This modulation method makes scanning broad spectral ranges to study radicals possible, instead of scanning line by line. This method is promising to study new radicals never observed previously. The revised vinoxy data set provides a more accurate set of molecular constants that includes transitions at higher frequencies, where $N''$ and $K_a''$ are up to 41 and 18 respectively. It improves the quartic centrifugal distortion by about 2 orders of magnitude, and some sextics are determined for the first time. This study may have implications for future detection of $CH_2CHO$ in hot environments of the interstellar medium and up to the THz range.

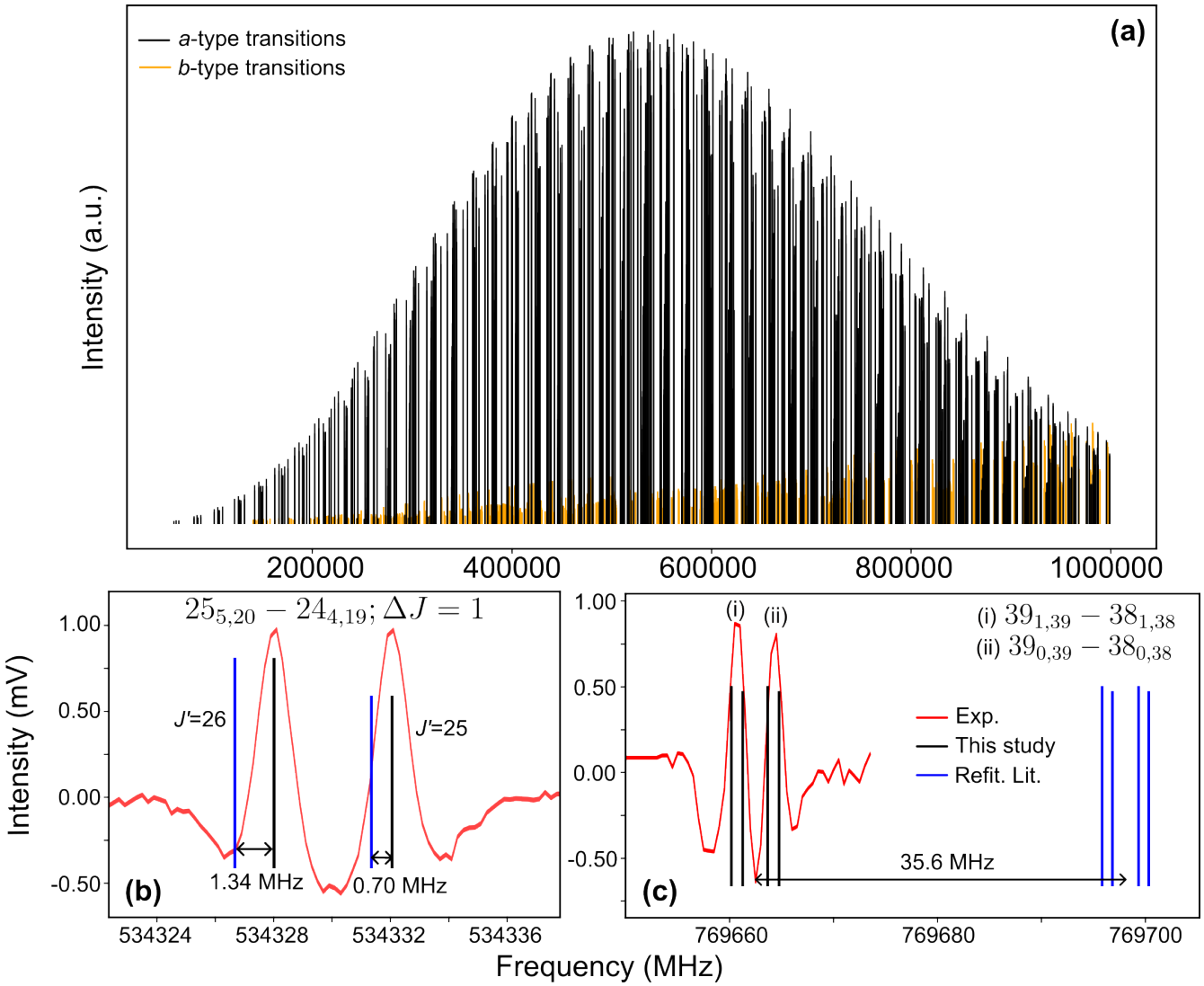


Figure 5: **Pure rotation spectrum of $CH_2CHO$ up to 1 THz at 225 K and comparison of the experimental measurements with models.** **(a)** Simulation of the spectrum of the vinoxy radical using the spectroscopic constants derived in this study at $T = 225$ K. $a$-type transitions are plotted in black and $b$-type transitions in orange. **(b)** Zoom around 534 GHz showing two transitions measured experimentally (in red) compared with the simulation using the new set of parameters (in black) and using the refit of the literature data[21,25] (in blue). **(c)** Zoom around 769 GHz showing two rotational transitions with no fine structure (the spin-rotation is not resolved). $N_{K_a,K_c}$ and $J$ quantum numbers are used to label the transitions.

# Acknowledgement

This work has been supported by the "Investissements d'Avenir" LabEx PALM (ANR-10-LABX-0039-PALM), the *Région Ile-de-France* through DIM-ACAV$^+$, the *Agence Nationale de la Recherche* (ANR-19-CE30-0017-01), and the *Programme National "Physique et Chimie du Milieu*

*Interstellaire*" (PCMI) of CNRS/INSU with INC/INP co-funded by CEA and CNES. Quantum chemical calculations were performed using HPC resources from the "Mésocentre" computing center of CentraleSupélec and École Normale Supérieure Paris-Saclay supported by CNRS and Région Île-de-France (http://mesocentre.centralesupelec.fr/). We thank Kyle Crabtree for useful discussions concerning the demodulation scheme of our set-up, Jean-Christophe Loison for the loan of the F reaction set-up, and Thérèse Huet for the loan of the audio-amplifier.

## Supporting Information Available

The list of experimental frequencies and all files relevant to the fit and spectral prediction (linelist, parameters, partition function) are available as ASCII files.

## References

(1) Hirota, E. *High-Resolution Spectroscopy of Transient Molecules*; Springer Series in Chemical Physics; Springer Berlin Heidelberg: Berlin, Heidelberg, 1985; Vol. 40.

(2) Walker, R. W. Free radicals in combustion chemistry. *Science Progress (1933- )* **1990**, *74*, 163–187.

(3) Hunziker, H.; Kneppe, H.; Wendt, H. Photochemical modulation spectroscopy of oxygen atom reactions with olefins. *Journal of Photochemistry* **1981**, *17*, 377–387.

(4) Endo, Y.; Tsuchiya, S.; Yamada, C.; Hirota, E.; Koda, S. Microwave kinetic spectroscopy of reaction intermediates: O+ethylene reaction at low pressure. *The Journal of Chemical Physics* **1986**, *85*, 4446–4452.

(5) Fu, B.; Han, Y.-C.; Bowman, J. M.; Leonori, F.; Balucani, N.; Angelucci, L.; Occhiogrosso, A.; Petrucci, R.; Casavecchia, P. Experimental and theoretical studies of the O( $^3$ P) + C $_2$ H $_4$

reaction dynamics: Collision energy dependence of branching ratios and extent of intersystem crossing. *The Journal of Chemical Physics* **2012**, *137*, 22A532.

(6) Occhiogrosso, A.; Viti, S.; Balucani, N. An improved chemical scheme for the reactions of atomic oxygen and simple unsaturated hydrocarbons – implications for star-forming regions. *Monthly Notices of the Royal Astronomical Society* **2013**, *432*, 3423–3430.

(7) Ramsay, D. A. Electronic Spectra of Polyatomic Molecules—A Brief Survey. *The Journal of Chemical Physics* **1965**, *43*, S18–S23.

(8) Inoue, G.; Akimoto, H. Laser-induced fluorescence of the C $_2$ H $_3$ O radical. *The Journal of Chemical Physics* **1981**, *74*, 425–433.

(9) Jacox, M. E. The reaction of F atoms with acetaldehyde and ethylene oxide. Vibrational spectra of the CH3CO and CH2CHO free radicals trapped in solid argon. *Chemical Physics* **1982**, *69*, 407–422.

(10) Heaven, M.; Dimauro, L.; Miller, T. A. Laser-induced fluorescence spectra of free-jet cooled organic free radicals. Vinoxy, cyclopentadienyl, and benzyl. *Chemical Physics Letters* **1983**, *95*, 347–351.

(11) DiMauro, L. F.; Heaven, M.; Miller, T. A. Laser induced fluorescence study of the $B\ ^2\ A - X\ ^2\ A$ transition of the vinoxy radical in a supersonic free jet expansion. *The Journal of Chemical Physics* **1984**, *81*, 2339–2346.

(12) Gejo, T.; Takayanagi, M.; Kono, T.; Hanazaki, I. Hole Burning Spectrum of the Vinoxy Radical in the B ($^2$A") State in a Supersonic Free Jet. *Chemistry Letters* **1993**, *22*, 2065–2068.

(13) Wan, R.; Chen, X.; Wu, F.; Weiner, B. R. Observation of new vibronic transitions in the B $^2$A"-X $^2$A" manifold of the $CH_2CHO$ radical. *Chemical Physics Letters* **1996**, *260*, 539–544.

(14) Brock, L. R.; Rohlfing, E. A. Spectroscopic studies of the B2A"-X2A" system of the jet-cooled vinoxy radical. *The Journal of Chemical Physics* **1997**, *106*, 10048–10065.

(15) Nagai, H.; Carter, R. T.; Huber, J. Spectroscopy and dynamics of selected rotational levels in the B $^2$A" state of the vinoxy radical. *Chemical Physics Letters* **2000**, *331*, 425–432.

(16) Alconcel, L. S.; Deyerl, H.-J.; Zengin, V.; Continetti, R. E. Structure and Energetics of Vinoxide and the X ($^2$A") and A ($^2$A') Vinoxy Radicals. *The Journal of Physical Chemistry A* **1999**, *103*, 9190–9194.

(17) Yacovitch, T. I.; Garand, E.; Neumark, D. M. Slow photoelectron velocity-map imaging spectroscopy of the vinoxide anion. *The Journal of Chemical Physics* **2009**, *130*, 244309.

(18) Thomas, P. S.; Chhantyal-Pun, R.; Kline, N. D.; Miller, T. A. The A-X absorption of vinoxy radical revisited: Normal and Herzberg–Teller bands observed via cavity ringdown spectroscopy. *The Journal of Chemical Physics* **2010**, *132*, 114302, Content: AX.

(19) Utkin, Y. G.; Han, J.-X.; Sun, F.; Chen, H.-B.; Scott, G.; Curl, R. F. High-resolution jet-cooled and room temperature infrared spectra of the $\nu_3$ CH stretch of vinoxy radical. *The Journal of Chemical Physics* **2003**, *118*, 10470–10476.

(20) Hansen, N.; Mäder, H.; Temps, F. Rotational Transitions of the CH2CHO Radical Detected by Pulsed Laser Photolysis–Molecular Beam–Fourier-Transform Microwave Spectroscopy. *Journal of Molecular Spectroscopy* **2001**, *209*, 278–279.

(21) Endo, Y.; Nakajima, M. Fourier-transform microwave spectroscopy of the vinoxy radical, CH2CHO. *Journal of Molecular Spectroscopy* **2014**, *301*, 15–19.

(22) Dupuis, M.; Wendoloski, J. J.; Lester, W. A. Electronic structure of vinoxy radical CH $_2$ CHO. *The Journal of Chemical Physics* **1982**, *76*, 488–492.

(23) Huyser, E. S.; Feller, D.; Borden, W. T.; Davidson, E. R. A theoretical study of the

acetaldehyde-derived radical. *Journal of the American Chemical Society* **1982**, *104*, 2956–2959.

(24) Endo, Y.; Hirota, E. The submillimeter-wave spectrum of the deuterated vinoxy radical, CD2CDO. *Journal of Molecular Spectroscopy* **1988**, *127*, 535–539.

(25) Endo, Y.; Saito, S.; Hirota, E. The microwave spectrum of the vinoxy radical. *The Journal of Chemical Physics* **1985**, *83*, 2026–2034, Content: Vinoxy.

(26) Neri, R. et al. NOEMA redshift measurements of bright Herschel galaxies. *ASTRONOMY & ASTROPHYSICS* **2020**, *635*.

(27) Partnership, A.; Brogan, C. L.; Pérez, L. M.; Hunter, T. R.; Dent, W. R. F.; Hales, A. S.; Hills, R. E.; et al. THE 2014 ALMA LONG BASELINE CAMPAIGN: FIRST RESULTS FROM HIGH ANGULAR RESOLUTION OBSERVATIONS TOWARD THE HL TAU REGION*. *The Astrophysical Journal Letters* **2015**, *808*, L3.

(28) Chai, J.-D.; Head-Gordon, M. Long-range corrected hybrid density functionals with damped atom–atom dispersion corrections. *Phys. Chem. Chem. Phys.* **2008**, *10*, 6615.

(29) Dunning, T. H. Gaussian basis sets for use in correlated molecular calculations. I. The atoms boron through neon and hydrogen. *J. Chem. Phys.* **1989**, *90*, 1007–1023.

(30) Woon, D. E.; Dunning, T. H. Gaussian basis sets for use in correlated molecular calculations. III. The atoms aluminum through argon. *J. Chem. Phys.* **1993**, *98*, 1358–1371.

(31) Frisch, M. J. et al. Gaussian 16 Revision A.01. 2016.

(32) Chitarra, Olivia; Martin-Drumel, Marie-Aline; Gans, Bérenger; Loison, Jean-Christophe; Spezzano, Silvia; Lattanzi, Valerio; Müller, Holger S. P.; Pirali, Olivier Reinvestigation of the rotation-tunneling spectrum of the CH2OH radical - Accurate frequency determination of transitions of astrophysical interest up to 330 GHz. *A&A* **2020**, *644*, A123.

(33) Coudert, L. H.; Chitarra, O.; Spaniol, J.-T.; Loison, J.-C.; Martin-Drumel, M.-A.; Pirali, O. Tunneling motion and splitting in the CH $_2$ OH radical: (Sub-)millimeter wave spectrum analysis. *The Journal of Chemical Physics* **2022**, *156*, 244301.

(34) Chitarra, O.; Pirali, O.; Spaniol, J.-T.; Hearne, T. S.; Loison, J.-C.; Stanton, J. F.; Martin-Drumel, M.-A. Pure Rotational Spectroscopy of the CH $_2$ CN Radical Extended to the Sub-Millimeter Wave Spectral Region. *The Journal of Physical Chemistry A* **2022**, *126*, 7502–7513.

(35) Amano, T.; Hirota, E. Microwave spectrum of the molecular oxygen in the excited vibrational state. *Journal of Molecular Spectroscopy* **1974**, *53*, 346–363.

(36) Pickett, H.; Poynter, R.; Cohen, E.; Delitsky, M.; Pearson, J.; Müller, H. SUBMILLIMETER, MILLIMETER, AND MICROWAVE SPECTRAL LINE CATALOG. *Journal of Quantitative Spectroscopy and Radiative Transfer* **1998**, *60*, 883–890.

(37) Western, C. M. PGOPHER: A program for simulating rotational, vibrational and electronic spectra. *Journal of Quantitative Spectroscopy and Radiative Transfer* **2017**, *186*, 221–242.

(38) Pickett, H. M. The fitting and prediction of vibration-rotation spectra with spin interactions. *Journal of Molecular Spectroscopy* **1991**, *148*, 371–377.

(39) Guelachvili, G. Selective detection of paramagnetic species by high-information Fourier-transform spectrometry. *Journal of the Optical Society of America B* **1986**, *3*, 1718.

(40) Lee, K. L. K.; McCarthy, M. Bayesian Analysis of Theoretical Rotational Constants from Low-Cost Electronic Structure Methods. *The Journal of Physical Chemistry A* **2020**, *5*, 898–910.